

**Supplemental Material:**  
**Variance-Minimizing Transport Plans for Inter-surface Mapping**

Manish Mandad

David Cohen-Steiner

Leif Kobbelt

Pierre Alliez

Mathieu Desbrun

ACM Trans. Graph. 36, 4, Article 39 (July 2017)

In this Supplemental Material we provide additional figures to complement the associated article, and also include larger versions of a few figures of the actual paper.

**1D Mapping.** Fig. 1 shows the transport plan after alternating minimization iterations for an example between two curves.

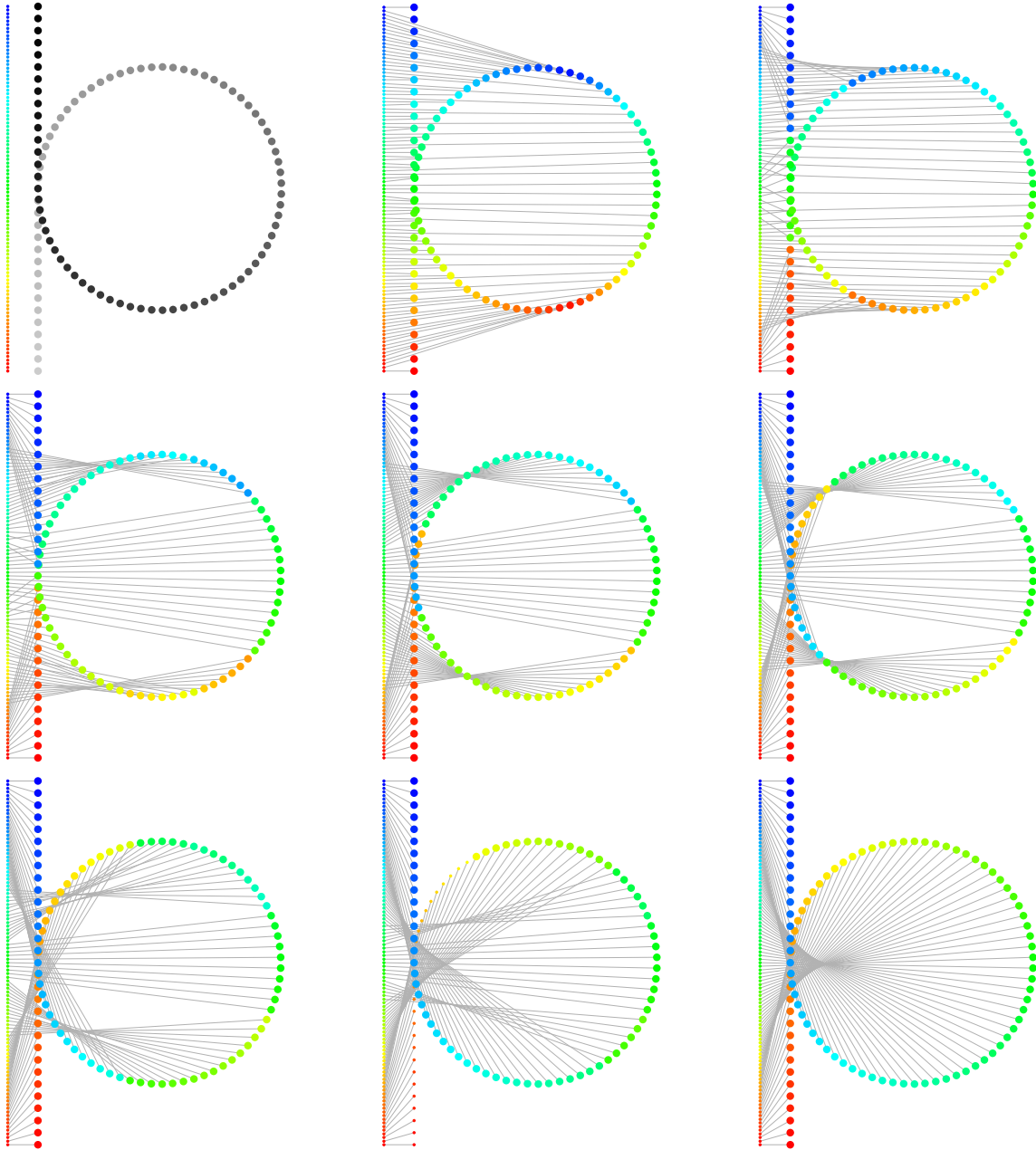


**Figure 1: Unfolding a curve.** A Gaussian weighting function is used as our local test function to measure geodesic variance.

**Isometric Exmples.** Fig. 2 shows a centaur from the TOSCA dataset [Bronstein et al. 2008] in three isometric poses. The maps are obtained without any user interaction and without area relaxation.

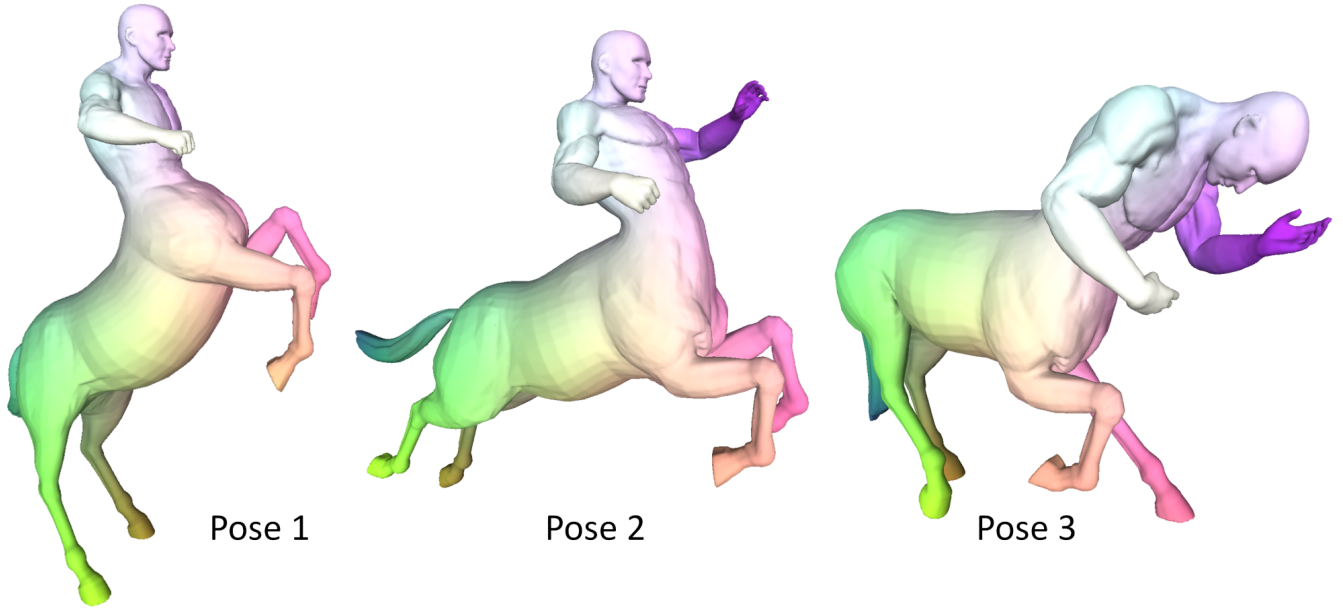


**Figure 2: Centaur in three isometric poses.** Dense maps are successfully established between three isometric poses of the centaur model. No user interactions were required, and no area relaxation was allowed.

Fig. 3 shows a dog in nine isometric poses. Initialization using the Wasserstein-2 term was not sufficient for all of them as the models are not rigidly-aligned, we thus used two user-specified constraints, one for the left hind leg and one for the front right leg, to avoid left/right flipping. Strip coloring of the source dog (left) is mapped onto the eight target dogs using the variance-minimizing transport plan computed by our algorithm.

**Non-isometric Exmples.** We challenge our algorithm in Fig. 4 by computing a map between two highly non-isometric models of genus 1: a torus and a kitten. As expected, the map gets highly non-conformal in this example; but the resulting map is valid and natural nonetheless.

Fig. 6 depicts a mapping between a man and the Homer model. Four constraints are specified, on each hand and each foot. As expected, the distortion is very large due to vast differences in shape, especially on the head and feet. However, our fully geometric map optimization leads to correspondences being well captured.

**Different Topology.** Fig.7 depicts a mapping between a sphere and three genus 1 surfaces with increasing size of handle.

**Ironing.** Finally, we show a more detailed example of ironing of a purposely defective map in Fig. 9. Note that ironing usually happens at very small scale, as soon as a flaw in the map is detected. However, the map shows a large scale discontinuity to demonstrate the robustness of this process.

## References

- BRONSTEIN, A., BRONSTEIN, M., AND KIMMEL, R. 2008. *Numerical Geometry of Non-Rigid Shapes*, 1 ed. Springer Publishing Company, Incorporated.
- KIM, V. G., LIPMAN, Y., AND FUNKHOUSER, T. A. 2011. Blended intrinsic maps. *ACM Trans. Graph* 30, 4, 79.

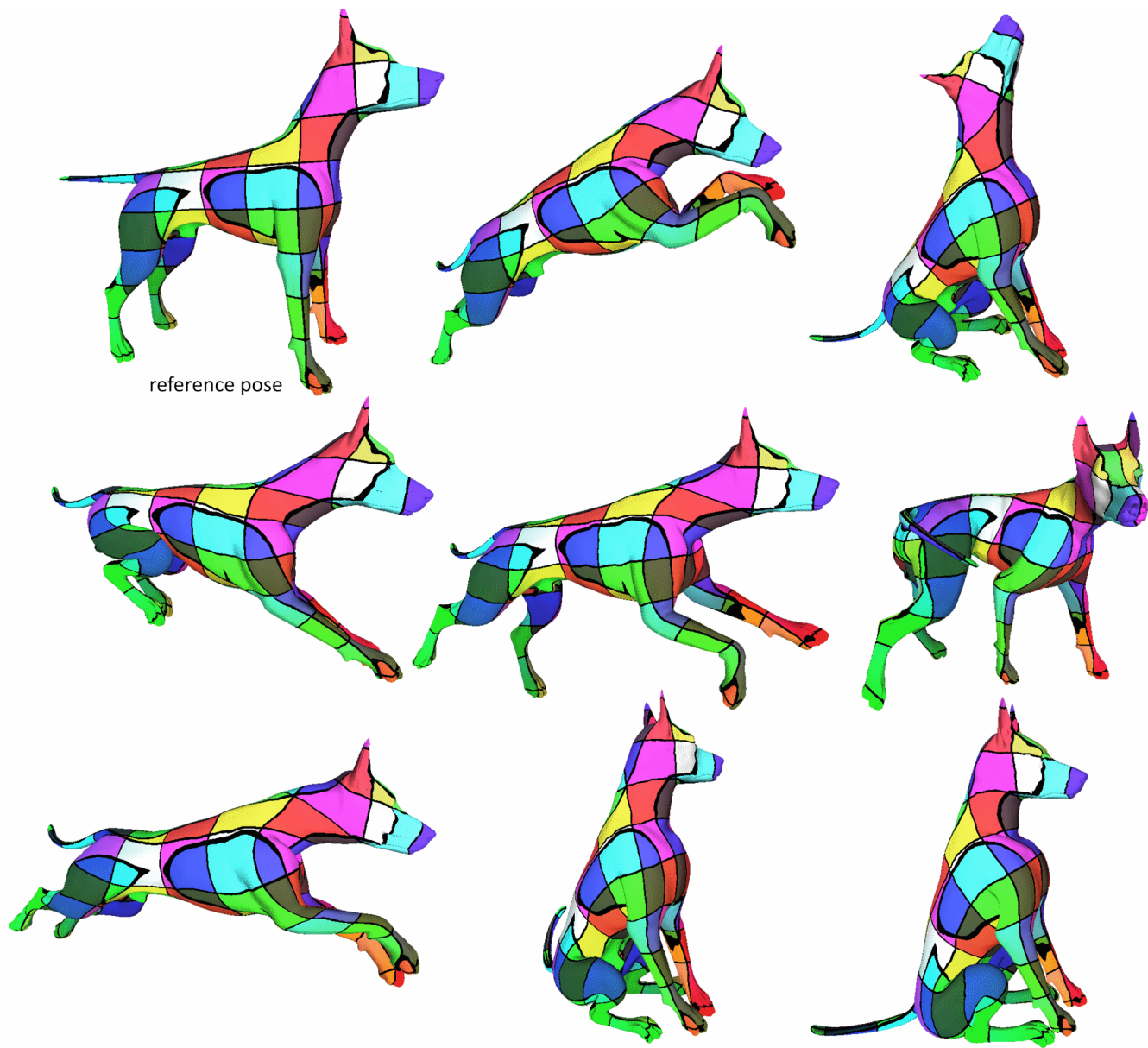


**Figure 3: Isometric deformation of a dog.** *Our approach successfully establishes proper dense maps between different isometric poses of a dog; the top left “neutral” pose is chosen as reference for coloring.*

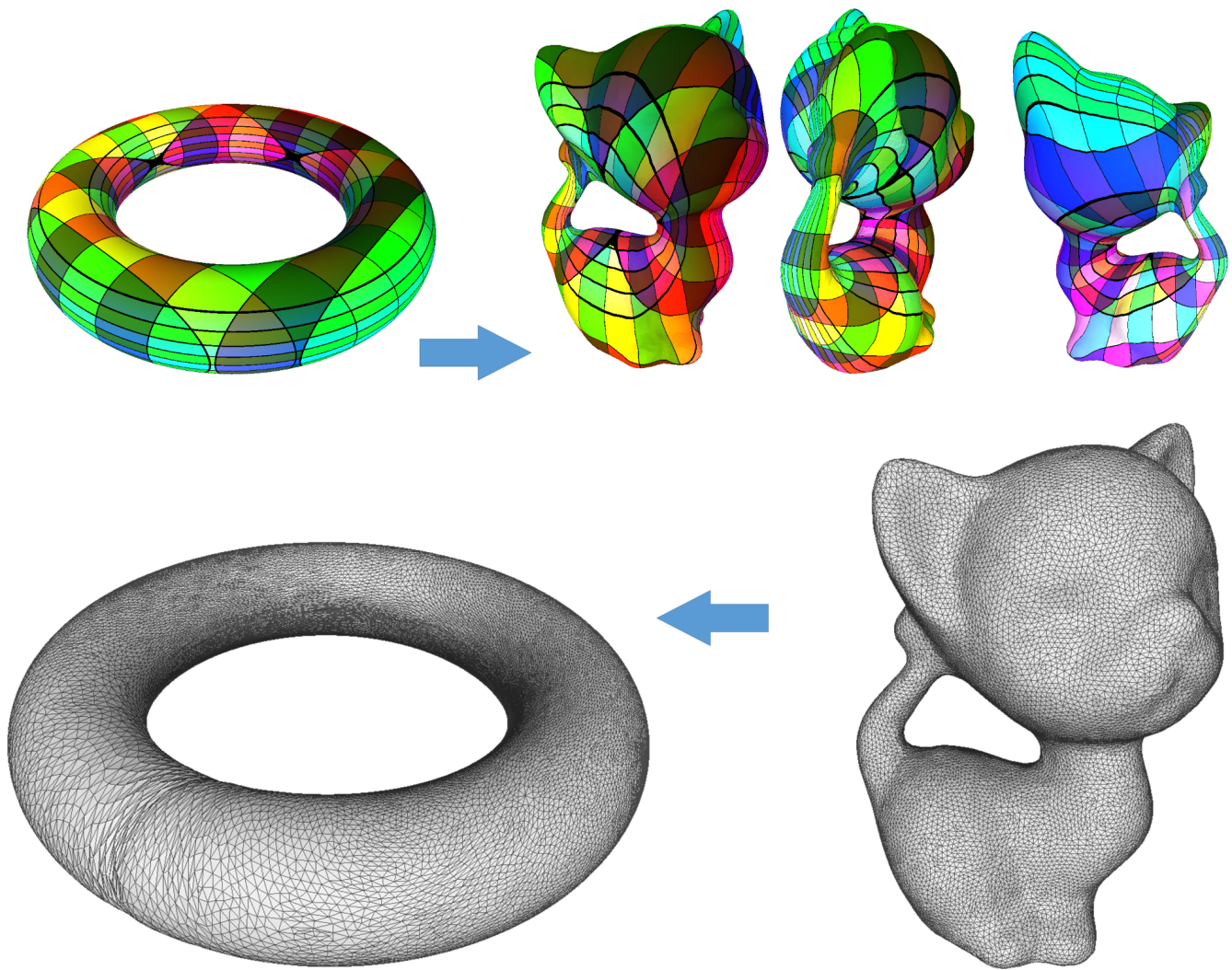


**Figure 4: Highly non-isometric mapping.** A torus is mapped to a kitten. Top: strip coloring on the torus mapped to the kitten. Bottom: kitten mesh relocated onto the torus.



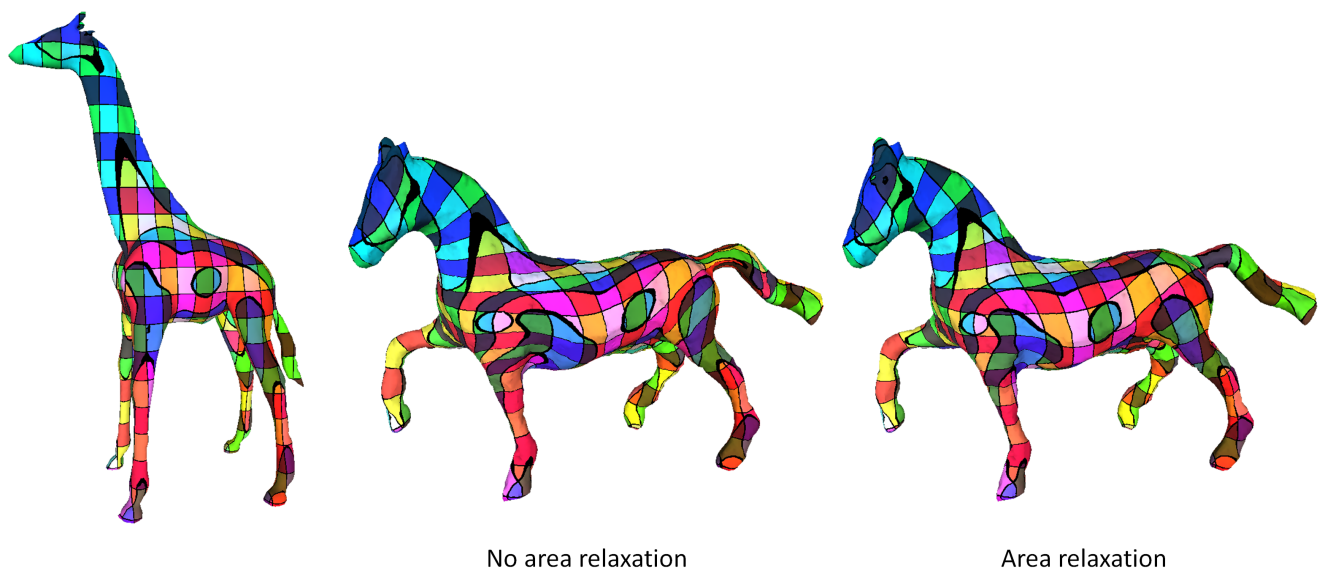


**Figure 5: Area vs. no area relaxation.** A giraffe is mapped to a horse. Conformality is significantly improved when area relaxation ( $D=2$ ) is activated, see in particular the front shoulders.

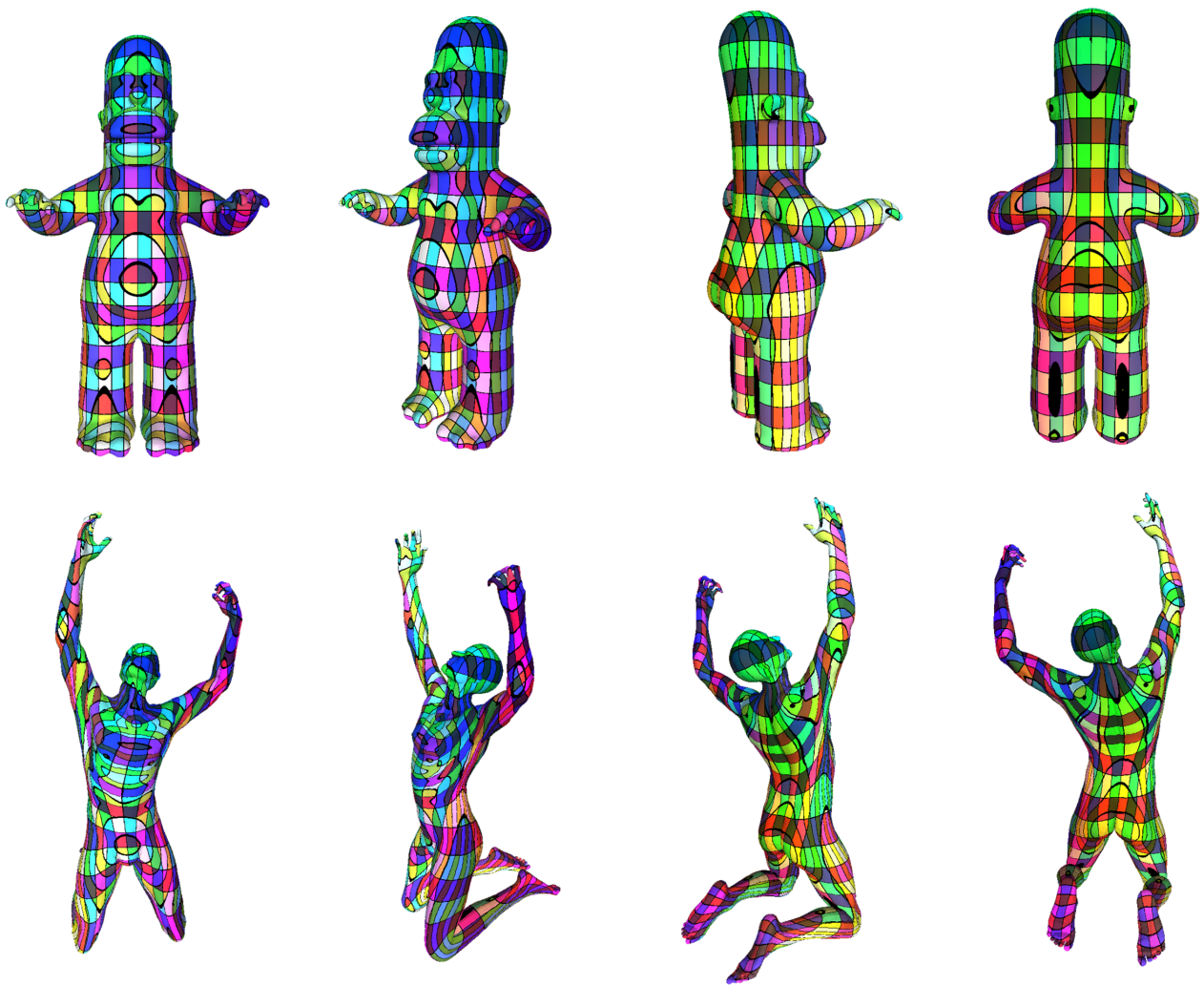


**Figure 6: Mapping a man to Homer.** *Doh! Even if the two models vary significantly, our automatic mapping computation succeeds in providing a natural map between the two.*

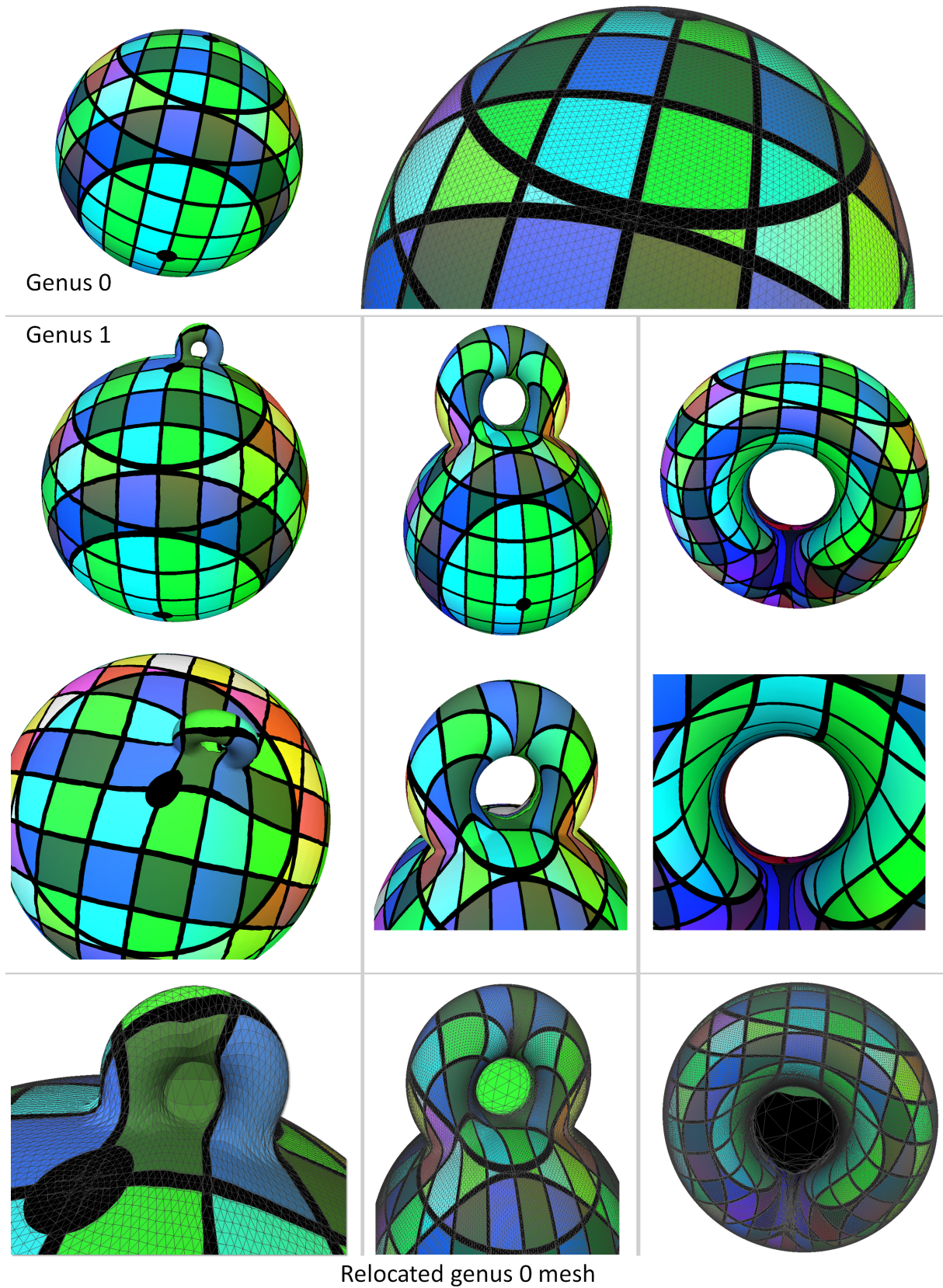


**Figure 7: Different topology.** *Top: a sphere and its strip coloring; Middle: a sphere with a small protruding handle, the same sphere with a larger handle, and then a regular torus are mapped to the top sphere. Maps for the sphere with handles are discontinuous, but only locally. The discontinuity for the torus to sphere is no longer local; nevertheless, the map is continuous over half of the sphere. Bottom: the sphere mesh is relocated onto the genus-0 surfaces.*

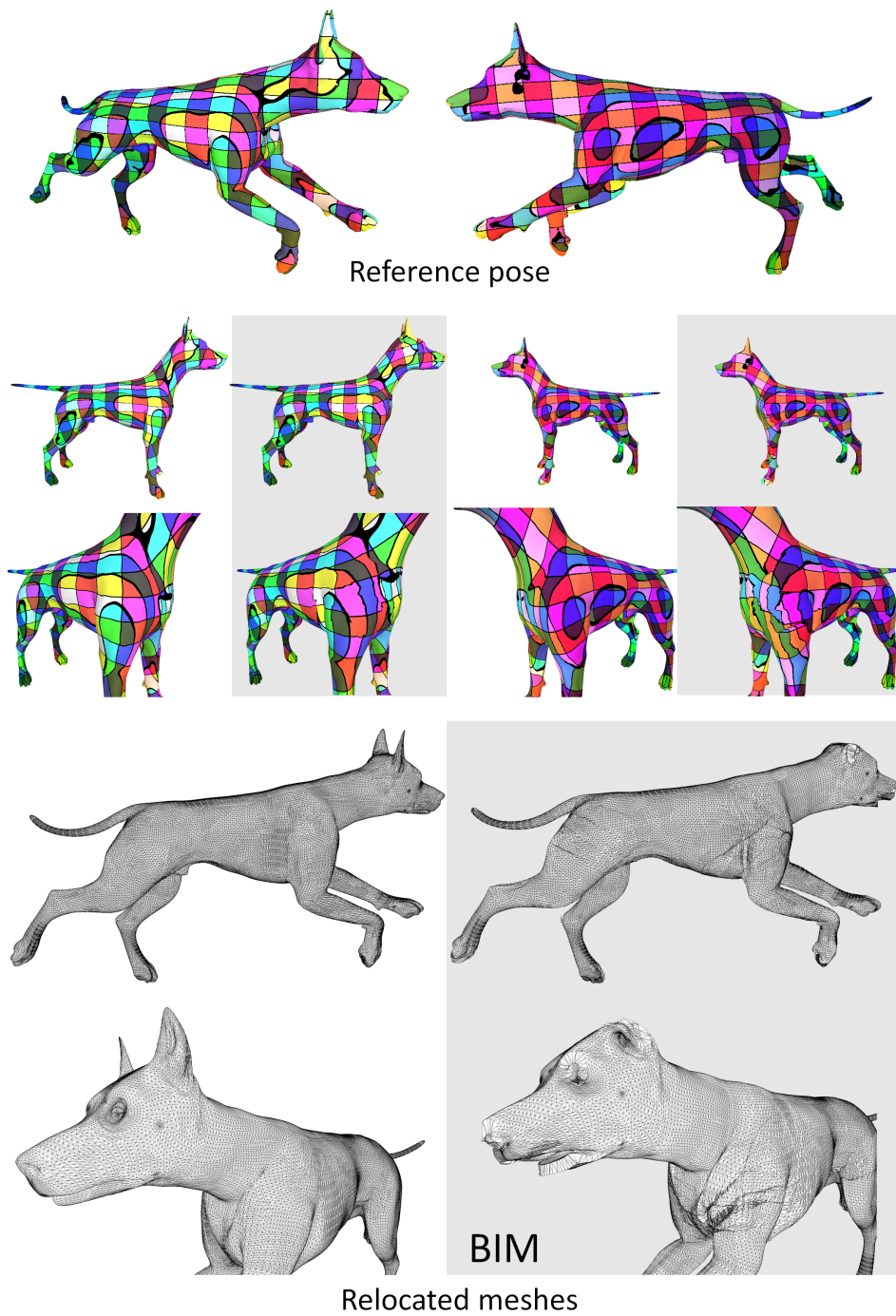


**Figure 8: Comparison with BIM.** The dog model is mapped to another isometric pose with no user-specified constraints. Grey background: results obtained with blended intrinsic maps (BIM [Kim et al. 2011]); the BIM map between these two isometric models is defective on the ears and shoulders. We also depict the meshes relocated via their respective maps to make the maps more obvious.



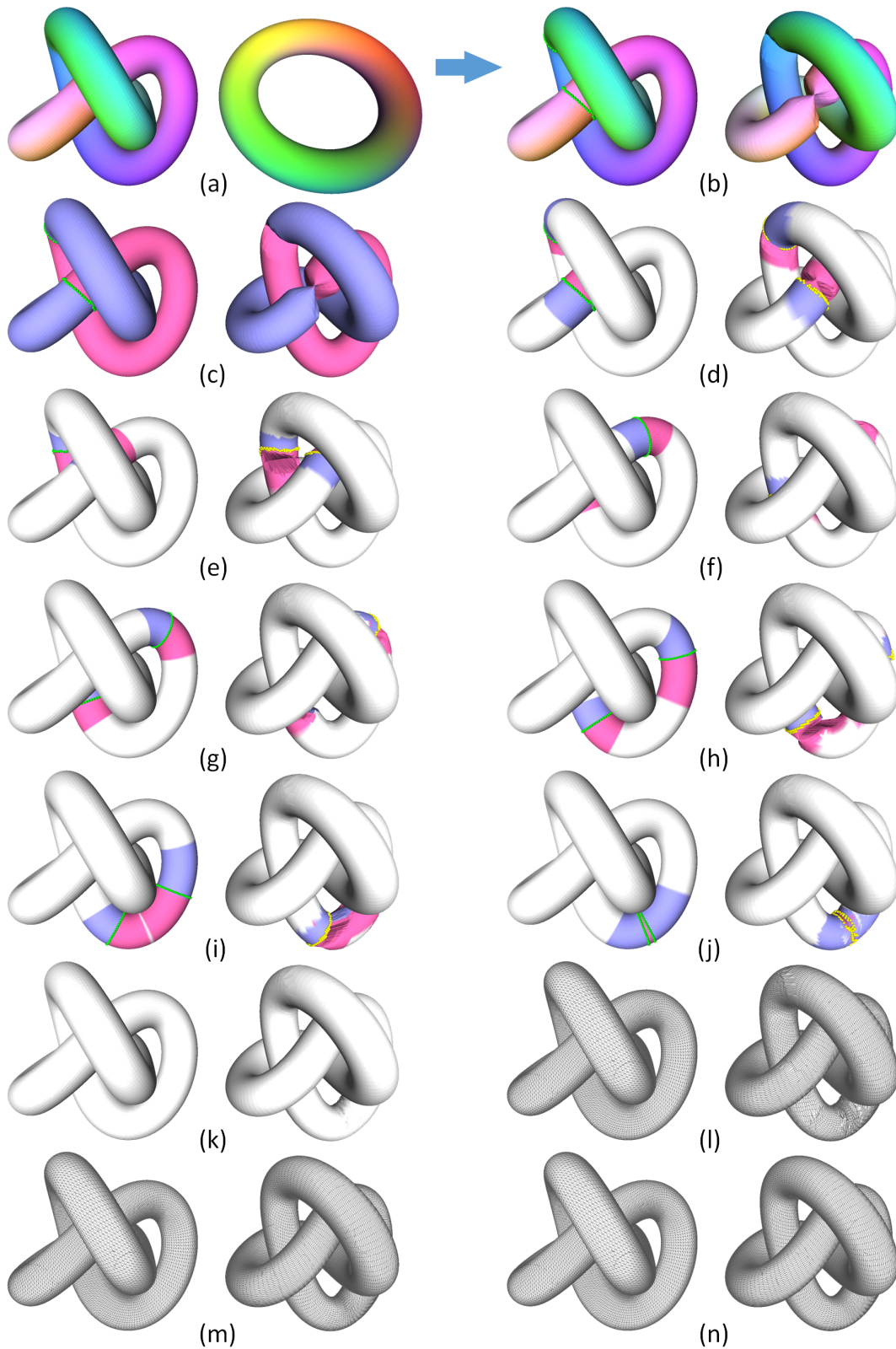


**Figure 9: Flip-fixing process.** Given a suboptimal map between a knotted torus and a torus (a), as clearly depicted through the relocated mesh of the torus (b), patches with consistent map orientation are found using tangent planes in diffusion space (two patches here depicted in blue and pink) (c). Ironing proceeds through front propagation depicted in green (the mapped front is depicted in yellow) to remove all artifacts (d – k). For each strip, blue indicates the visited parts while the non-visited parts are in pink. In case of multiple fronts, each front is considered independently. Ironing is followed by a few alternating minimization iterations on the whole data leading to a smooth final map without discontinuities (l – n). Note that this example is only for illustration purposes; ironing is only happening at small scales in practice as we continuously and preemptively test the validity of the map throughout our optimization stages.